Master's Thesis of Material Science and Engineering

A tensile-dominated multi-directional auxetic deformation of 3D fiber woven structure

一种拉伸主导多方向拉胀变形的三维纤维编织结构

August 2022

Seoul National University

Department of Materials Science and Engineering

Yuze Li

A tensile-dominated multi-directional auxetic deformation of 3D fiber woven structure

Advisor: Woong-Ryeol Yu

by

Yuze Li

2022

Department of Materials Science and
Engineering Graduated School Seoul
National University

A tensile-dominated multi-directional auxetic deformation of 3D fiber woven structure

Name of Examiner: Woong-Ryeol Yu

Submitting a master's thesis of
Material Engineering

August 2022

Graduate School of Department of
Materials Science and Engineering
Seoul National University

Yuze Li

Confirming the master's thesis written by
Yuze Li
August 2022

Chair	Cheol-Hee Ahn	(Seal)
Vice Chair	Woong-Ryeol Yu	(Seal)
Examiner	Myoung-Gyu Lee	(Seal)

Abstract

Previous discussions on auxetic composites reinforced with woven fiber structures have focused on unidirectional tension or compression, and often require multiple fibers to play different roles in the structure, making it difficult to perfectly exploit the advantages of auxetic materials in real-world applications. We present here a woven structure that can be stretched in multiple directions to produce an auxetic behavior. The single-layer structure was successfully fabricated by three dimensions (3D) printing method and compared by the finite element analysis (FEA). Also, the multi-directional tensile deformation behavior of the 3D structure was simulated, and the Poisson's ratio (PR) values of the single-layer structure and the 3D structure were obtained. Moreover, the factors affecting the auxetic behavior of the structure were discussed. The results show that the experimental results have a good similarity with the FEA results, and the structure can achieve the auxetic behavior when stretched in all three directions. In particular, the diameter ratio of the fibers in each direction is an influential factor in the extent of auxetic deformation of the structure. This study provides a new approach to the development of multi-directional auxetic fiber composites. In addition, it reveals the potential of multi-directional auxetic materials for impact resistance performance applications.

Keywords ： Auxetic textile structure, Finite element analysis, Multi-dimensional auxetic deformation, 3D printing, Impact resistance

Student Number：2020-27841

List of Tables

List of Figures

Figure 9 Deformation behavior of 3D structure with Z-directional stretching. (a) A 3D structure and simulated Unit-2 deformation and (b) simulated Poisson's ratio according to displacement in the Z-direction.

Figure 10 Simulated deformation behavior of 3D structure with X- and Z-directional stretching when (a) ΦX(4 mm): ΦZ(5 mm) = 0.8:1, (b) ΦX(6 mm): ΦZ(5 mm) = 1.2:1. FE simulation of the measured PR with variation in the diameter ratio on stretching displacement (c) in the X and (d) Z directions.

Figure 11 Model geometry for simulated impacts.

Figure 12 Results after PPR and NPR rigid body breakdown models.

Figure 13 During rigid body impact processes, both PPR and NPR models results of the relationship between the rigid body displacement and (a)velocity, (b)energy loss, (c)schematic diagram of the model for special events.

Chapter 1. Introduction

Auxetic materials have attracted much attention from researchers due to their unique behavior, as they possess a negative Poisson's ratio (NPR) [1]. In contrast to conventional materials, auxetic materials expand laterally when stretched axially, and contract laterally when compressed axially. This unique deformation also gives rise to excellent mechanical properties, such as indentation resistance [2, 3], enhanced energy absorption [4, 5], increased shear stiffness [6], and negative thermal expansion [7, 8]. Based on these properties, auxetic materials also hold great promise for applications in aerospace, sensors, biomedical machinery, and protective devices, etc. [9-14].

Since the introduction of the dilatational lattice structure by Gibson et al. in 1982 [15], a large number of auxetic metamaterials have been designed and manufactured. According to the deformation mechanism, auxetic metamaterials are classified mainly into chiral structures [16, 17], rigid rotational structures [18], and re-entrant structures [19, 20], etc. Composites with NPR behavior, achieved by embedding inclusions of different geometries, are also now coming into view. Some inclusion designs include a rigid rotating square, and triangular, rhombohedral, spherical, and cubic structures [21-27]. However, as the application of composite materials has become more widespread, auxetic composites fabricated with high-performance fibers have often proven effective in solving the auxetic lattice structure stiffness and strength problems associated with the bendingdominated deformation mechanism.

There are two approaches for fabricating auxetic composites with fibers. The first is the usage of non-auxetic materials, for which a pre-preg structure is stacked to achieve NPR behavior of the laminates [28, 29]. However, the intrinsic structure is limited to a certain extent, and the requirement for individual layers to be highly anisotropic also means that auxetic behavior of the composite can only be expressed in one direction [30-32]. The second method for achieving auxetic behavior of the composite material under compression or tension is to use a specially designed fiber weave. For instance, well-known auxetic yarn and fabric designs rely on the diameter differences of fibers [33], multi-layer orthogonal structures [34-37], and the addition of binder fibers [38], which often have the advantages of high strength and lightweight. However, composite materials fabricated using this method often require multiple fibers, each of which has unique properties and plays a different role, resulting in a complex fabrication process. In addition, the two-dimensional (2D) and three-dimensional (3D) structures fabricated by the second method exhibit anisotropy. Moreover, the restriction in direction of load imposition to attain auxetic behavior invariably limits the potential applications of the auxetic material. At present, none of the 3D woven structures reported in the literature exhibit auxetic behavior when tensile loads are applied in multiple directions.

In this study, two units that can create auxetic deformation when stretched in different directions were designed based on the consideration of continuous manufacturing and structural stability. Then, the two units were arranged by staggered connection to finally form a new 3D auxetic woven structure that can be stretched in multiple directions with the same type of fiber. The 2D single-layer structure was fabricated by 3D printing, and its tensile deformation behavior in three directions was investigated. The finite element (FE) analysis was also performed and compared with the experimental results, while the multi-directional deformation behavior of the 3D structure was simulated. In order to understand the factors influencing the NPR behavior of the structure, simulations were carried out to calculate the tensile behavior and auxetic performance of the structure with different fiber elastic modulus, and different fiber diameter ratios in the three directions. Inspired by the ballistic applications of multi-layer fabrics [39], finally we provided predictions for the potential of multi-directional auxetic material for impact resistance.

Chapter 2. Design and modeling

2.1 New design of auxetic 3D textile structure

The particular negative Poisson's ratio effect of fiber assembly is due to its unique three-dimensional structural design, which makes the three directions of the fiber weaving route a key point to achieving the overall structure realizing the auxetic behavior. First of all, in order to design a structure that can realize the auxetic behavior in X and Y directions, the X- and Y-direction fibers need to be bent while maintaining symmetry, and the Z-direction fibers play a role in securing the unit, forming the unit one pattern as shown in Figure 1(a). It will cause the same deformation result when the unit one structure is stretched in X or Y direction due to the symmetry of the structure. Where, unit one does not deform when it is stretched in the Z direction. Thus, in order to achieve multi-directional structural auxetic behavior, it becomes necessary for the existence of unit two that does not deform when stretched in the X and Y directions and produces auxetic behavior when stretched in the Z direction. As shown in Figure 1(a), the unit two mold sample is designed with the Z-direction fibers bent and the X- and Y-direction fibers play a fixed role.

Next, taking X-directional stretching as an example, after the X-direction fibers are stretched, they become straight from bending, and the X-direction fibers originally next to each other in the center will be separated, resulting in a gap in the middle, and the two Z-direction fibers arranged in the Y direction are moved to both sides by the force. Affected by the influence of the unit boundary, the Y-direction fibers are also deformed in the same way by tension, forming the unit one deformation as shown in Figure 1(b). When unit two is stretched in the Z direction, the Z-direction fibers are straightened by the force leading to a gap in the middle, and the X- and Y-direction fibers move outward leading to an increase in the strain of unit two in the XY plane, as shown in the schematic diagram of unit two deformation in Figure 1 (c).

Following, to realize the auxetic behavior of the 3D structure, this study selects the arrangement that the same unit is not connected regardless of the direction, which also makes the 3D structure, regardless of the size, will be composed of two different layers, such as Figure 1(d) layer one, layer two structure. This also results in unit one being the dominant unit when the stretching of the 3D structure in the X and Y directions, and unit two being the dominant unit in the stretching of the Z direction. At the same time, considering the necessity of continuous production and the structural stability of single fiber manufacturing, two units of X-directional fibers and Y-directional fibers are arranged in different order at the top and bottom, and are connected to form an interwoven mesh weave, finally forming a 3×3×4 3D structure schematic in Figure 1(e). It is worth mentioning that the geometric parameters of the designed structure include ΦX, ΦY and ΦZ, where ΦX is always equal to ΦY in this study in order to maintain the XY plane symmetry of the structure.

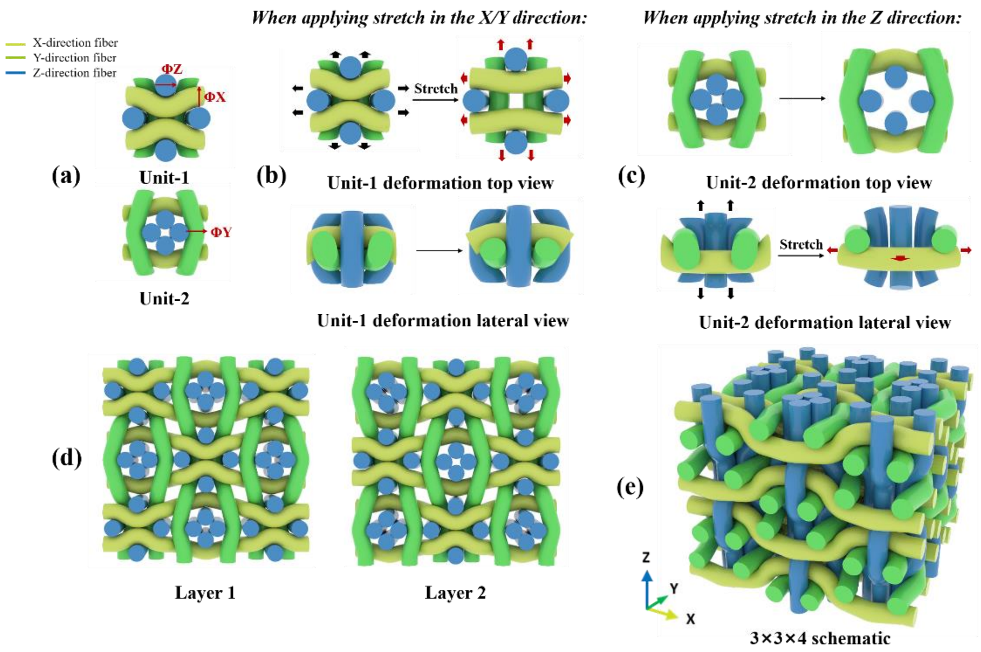

Figure 1. Three-dimensional (3D) structural design: (a) two units (Unit-1 and Unit-2), (b) Unit-1 deformation when stretched in X- or Y- direction, (c) Unit-2 deformation when stretched in the Z-direction, (d) two layers consisting of Unit-1 and Unit-2, and (e) a schematic diagram of a 3 × 3 × 4 3D structure.

2.2 Finite element modeling

As the manufacturing technology is relatively complex, and the internal deformation mode of the structure is difficult to observe. Therefore, the computational model can be very effective in estimating the deformation process of the structure and obtaining relatively accurate results as a way to verify the predicted structural auxetic behavior. In this study, one-layered (2D case) and 3×3×4 structures (3D case) with dimensions ΦX=ΦY=ΦZ=5 mm were modeled in CATIA software. For minimizing the boundary effect and promoting convergence, in the modeling, all the fibers in each direction in all models were increased by 5 mm parallel at both sides except for the Z-direction fibers in the 2D simulation of the layer one structure. Then imported into ABAQUS software for FEA, and all of them were subjected to standard static analysis. In the 2D structural analysis, the material of fibers was assumed to be isotropic and hyperelastic which was defined by the experiment of material's property test. In order to simulate the experimental stretching process, the static friction coefficient of interaction was set to 0.26, and the boundary conditions were set as shown in Table 1 and 2 for 2D structure. When performing the X-direction stretching simulation (Table 1), the Y-direction fibers' ends and the Z-direction fibers' bottom were fixed. Parallel 2 mm displacement was performed for both ends of the X-direction fibers only at the same time. As for the Z-direction stretching simulation (Table 2), the ends of the X- and Y-direction fibers, as well as the bottom of the Z-direction fibers, were fixed. Only the upper boundary in the Z direction was stretched 4 mm in parallel. After preliminary mesh convergence study, the mesh size was set to 1.2mm.

In the 3D structure analysis, unlike the 2D structure, the material property types were assumed to be isotropic and elastic, and Young's modulus is analyzed statically at 50 MPa, 100 MPa, and 200 MPa values to investigate the relationship between the material's own modulus and deformation of the structure. The boundary conditions were shown in Table 3 and 4. Whenever the stretching was applied in the X direction (Table 3) or Z direction (Table 4), the ends of the fibers in the tensile direction were set with 2 mm displacement at each side edge, and the ends of the fibers in the remaining directions were fixed to obtain the internal structural changes of the material. In addition, 3D structural models varying the diameter ratios ΦX (4 mm): ΦZ (5 mm) = 0.8:1 and ΦX (6 mm): ΦZ (5 mm) = 1.2:1 were modeled and analyzed as well, with the material Young's modulus set to 50 MPa, which will better comprehend the relationship between the diameter ratios of the fibers in the three directions on the deformation behavior of the structure.

The node selection carried out for the calculation of PR was shown in Figure 2(a). The displacement of nodes A and B in the X direction and the displacement of nodes C and D in the Y direction were output for the calculation of the X-direction stretching strain (ε_x) and the Y-direction strain (ε_y), respectively, for the X-direction stretching simulation of 2D structures. The Z-direction strain (ε_z) was determined by $\varepsilon_z = ({l_{z_0}}' - l_{z_0})/l_{z_0}$ when the 2D structure was simulated stretched in the Z direction, where l_{z_0} was the original height of the 2D structure and ${l_{z_0}}'$ was the height after stretching, determined by the displacements of the output nodes G and H in the Z direction. The Y-direction strain (ε_y') was identified by $\varepsilon_y' = ({l_{y_1}}' - l_{y_1})/l_{y_1}$, where l_{y_1} was the original distance between the X-direction fibers with the largest variation in displacement at the edge of the structure, and ${l_{y_1}}'$ was the distance after deformation, as determined by the displacements of the output nodes E and F in the Y direction. Then the Poisson's ratio (v) of the 2D structure when stretched in the Z direction was determined by

$v = -(\varepsilon_y/\varepsilon_z)$. The 3D structure was calculated by adopting the middle layer 1 structure in the X-direction stretching simulation. And when the PR calculation of the 3D structure stretched in the Z direction is performed, the height in the Z direction was different from that of the 2D structure, as shown in Figure 2(b). The stretching strain in the Z direction ($\varepsilon_z{}'$) was determined by $\varepsilon_z{}' = (l_{z_1}{}' - l_{z_1})/l_{z_1}$, where l_{z_1} was the original height of the original 3D structure and $l_{z_1}{}'$ was the stretching alteration height, which was determined by the output nodes I and J. Similarly, the intermediate layer one was selected to determine the Y-direction strain ($\varepsilon_y{}'$). The PR (v) of the final 3D structure when stretched in the Z direction was determined by $v = -(\varepsilon_y{}'/\varepsilon_z{}')$. In addition, on account of the symmetry of the structure in the XY plane, the auxetic behavior and PR values obtained by stretching in the X direction were equivalent to those of the Y direction for both 2D and 3D structures, and only representative simulation experiments in the X direction were conducted in this study.

Table 1. Boundary condition of layer 1 when stretching in the X-direction

	X-direction (mm)	Y-direction (mm)	Z-direction (mm)
X-directional fiber	$U_1^+ = 2,\ U_1^- = -2$	$U_2^+ = U_2^- = 0$	$U_3^+ = U_3^- = 0$
Y-directional fiber	$U_1^+ = U_1^- = 0$	$U_2^+ = U_2^- = 0$	$U_3^+ = U_3^- = 0$
Z-directional fiber	$U_1^+ = U_1^- = 0$	$U_2^+ = U_2^- = 0$	$U_3^- = 0$

Table 2. Boundary condition of layer 1 when stretching in the Z-direction

	X-direction (mm)	Y-direction (mm)	Z-direction (mm)
X-directional fiber	$U_1^+ = U_1^- = 0$	$U_2^+ = U_2^- = 0$	$U_3^+ = U_3^- = 0$
Y-directional fiber	$U_1^+ = U_1^- = 0$	$U_2^+ = U_2^- = 0$	$U_3^+ = U_3^- = 0$
Z-directional fiber	$U_1^+ = U_1^- = 0$	$U_2^+ = U_2^- = 0$	$U_3^+ = 4,\ U_3^- = 0$

Table 3. Boundary condition of the 3 × 3 × 4 structure when stretching in the X-direction

	X-direction (mm)	Y-direction (mm)	Z-direction (mm)
X-directional fiber	$U_1^+ = 2,\ U_1^- = -2$	−	−
Y-directional fiber	$U_1^+ = U_1^- = 0$	$U_2^+ = U_2^- = 0$	$U_3^+ = U_3^- = 0$
Z-directional fiber	$U_1^+ = U_1^- = 0$	$U_2^+ = U_2^- = 0$	$U_3^+ = U_3^- = 0$

Table 4. Boundary condition of the 3 × 3 × 4 structure when stretching in the Z-direction

	X-direction (mm)	Y-direction (mm)	Z-direction (mm)
X-directional fiber	$U_1^+ = U_1^- = 0$	$U_2^+ = U_2^- = 0$	$U_3^+ = U_3^- = 0$
Y-directional fiber	$U_1^+ = U_1^- = 0$	$U_2^+ = U_2^- = 0$	$U_3^+ = U_3^- = 0$
Z-directional fiber	−	−	$U_3^+ = 2,\ U_3^- = -2$

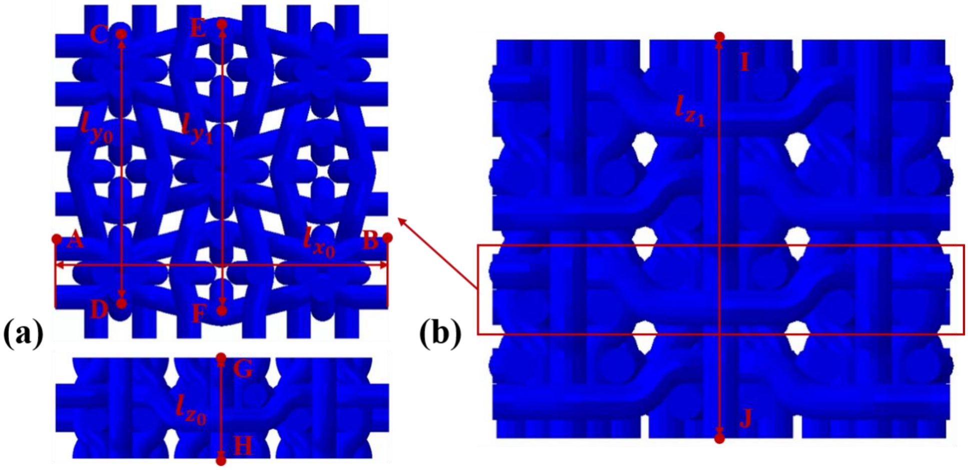

Figure 2. (a) Two-dimensional (2D) and (b) 3D modeling of the new auxetic structure for finite element analysis (FEA).

Chapter 3. Experimental

3.1 Materials

To verify the deformation behavior of the designed structure, the developed 3D auxetic structure was manufactured by using an LCD 3D printer (LM1, Carima, Korea). The polymer used was polyurethane (No.CUE05C UV resin) developed by Carima. First, the mechanical properties of the material were tested before the auxetic structure was fabricated. Four dog bone-shaped tensile specimens were printed and tested according to ISO 37:2017 standard, as shown in Figure 3(a). The uniaxial tensile experiments of the 4 printed specimens were performed at a rate of 100 mm/min using the universal machine (Quasar 5, Galdabini, Italy). The obtained engineering stress-strain curves are shown in Figure 3(b). And then, the average data of the four testing sets with strains less than 50% were taken and directly imported into the ABAQUS software to determine the elastomeric material's properties of hyperelastic. In addition, the material's own Poisson's ratio (PR) of 0.35 and static friction coefficient of 0.26 was provided by the supplier for reference.

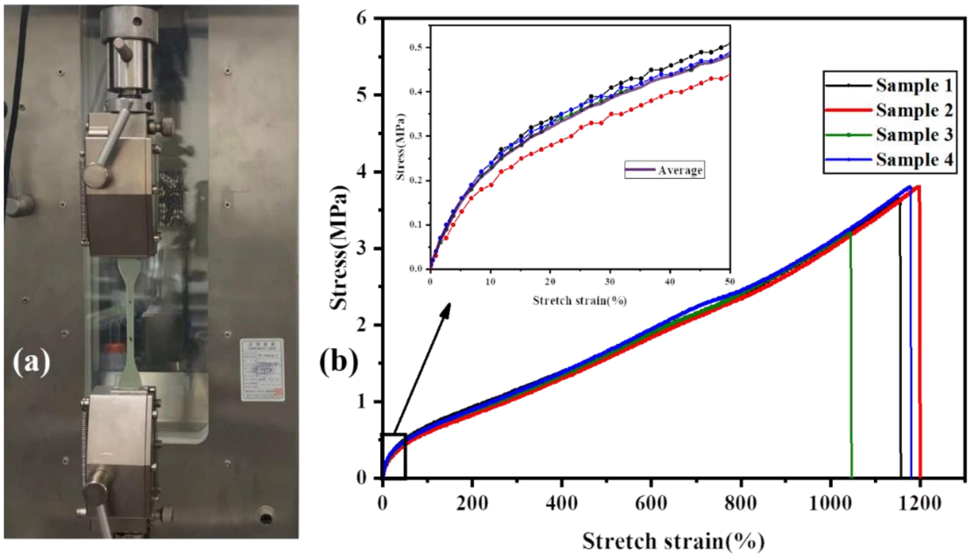

Figure 3. (a) Static tensile testing of polyurethane material used in this study and (b) stress–strain curves.

3.2 Manufacture of auxetic structures using 3D printing

Figure 4(a) shows the structure, with accurate dimensions of ΦX = ΦY = ΦZ = 5 mm modeled using CATIA software and imported into CarimaSlicer software. Given that the printing method is layer by layer, the printer cannot generate parts that are not supported in free space; thus, it is necessary to add support polymer to ensure the integrity of the sample. After setting the slicing parameters, the auxetic structure was printed using the 3D printer (see Figure 4(b)), and the excess support polymer was removed. The final sample was developed by drying at 405 nm under ultraviolet irradiation for 2 h.

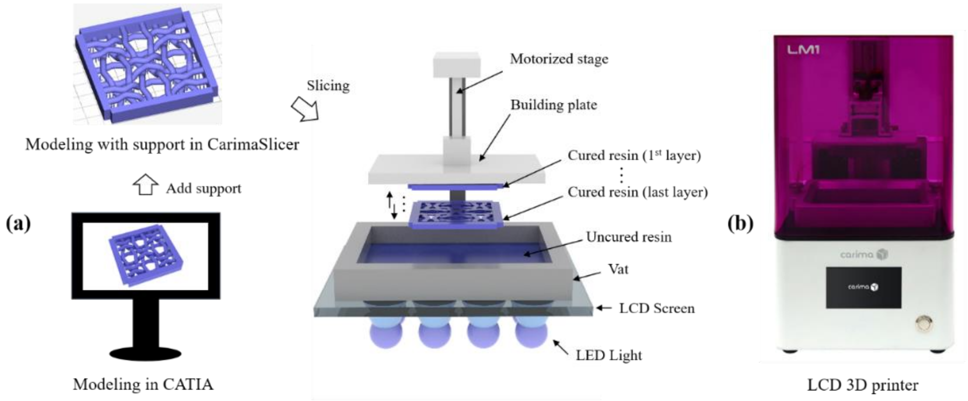

Figure 4. 3D printed textile structure: (a) schematic diagram of liquid crystal display 3D printing process, (b) Carima 3D printer.

3.3 Tensile characterization of auxetic structures

In order to evaluate the tensile behavior and performance of the structure, as well as to observe the integrity of the deformation process, tensile experiments (2D) in the X or Y direction were executed the 2D auxetic structure and Poisson's ratio data were compared with FE simulations. Due to the symmetry of the structure, the auxetic behavior in the X direction is the same as that in the Y direction, thus only the deformation of the tensile structure in the X direction is represented in the experimental tests. To facilitate the stretching and ensure the parallelism of the forces, and to give the structure sufficient space for deformation. Therefore, before the test, we printed 5 mm extensions on the ends of the fibers in the X and Y directions respectively and added a rectangular body of size 70 mm×5 mm×14 mm as the tensile part, and a base of size 70 mm×70 mm×10 mm at the bottom of the fibers in the Z direction to ensure the stability of the structure after assembly. Afterward, two tensile handles were printed using the NO.3DK83G rigid material developed by Carima to exactly match the dimensions of the machine and the stress applied to the structure.

The stretching machine, as shown in Figure 5(a), has two metal handles that can be moved, always in opposite directions of movement. And through the console of the machine, the speed and direction of stretching can be controlled. Firstly, the bottom of the printed sample was fixed on the machine, and the rigid handle was connected to the sample and the machine. Then set the machine running speed to 1 mm/min, and every 15 seconds, measure and record the displacement change of the center marker points of the furthest away Z-direction fibers in the Y direction with a vernier caliper, and do parallel ten sets of experiments. Finally, the average displacement data and PR results were calculated. The displacement variations were measured between the X-direction fiber edges ($l_{x_0}{}'$) and between the most varying fringe points, that is, Z-direction fibers at the very edge of the structure ($l_{y_0}{}'$). As shown in Figure 5(b), the X-direction tensile strain (ε_x) is calculated by $\varepsilon_x = (l_{x_0}{}' - l_{x_0})/l_{x_0}$, and the Y-direction strain (ε_y) is calculated by $\varepsilon_y = (l_{y_0}{}' - l_{y_0})/l_{y_0}$. Where l_{x_0} and l_{y_0} are the original distances of the structure, and $l_{x_0}{}'$ and $l_{y_0}{}'$ are the distances of the structure after stretching. Then the PR (v) of the 2D structure when stretched in the X direction is determined by $v = -(\varepsilon_y/\varepsilon_x)$.

To enable observation of the deformed process of the structure when stretched in the Z direction, nine fine needles with a length of 150 mm were used to pass parallel to the top of the Z-direction fibers, stretched upward, and photographed from above to observe the deformation behavior. This can effectively guarantee the parallel upward stretching force and obtain the deformed structure pattern.

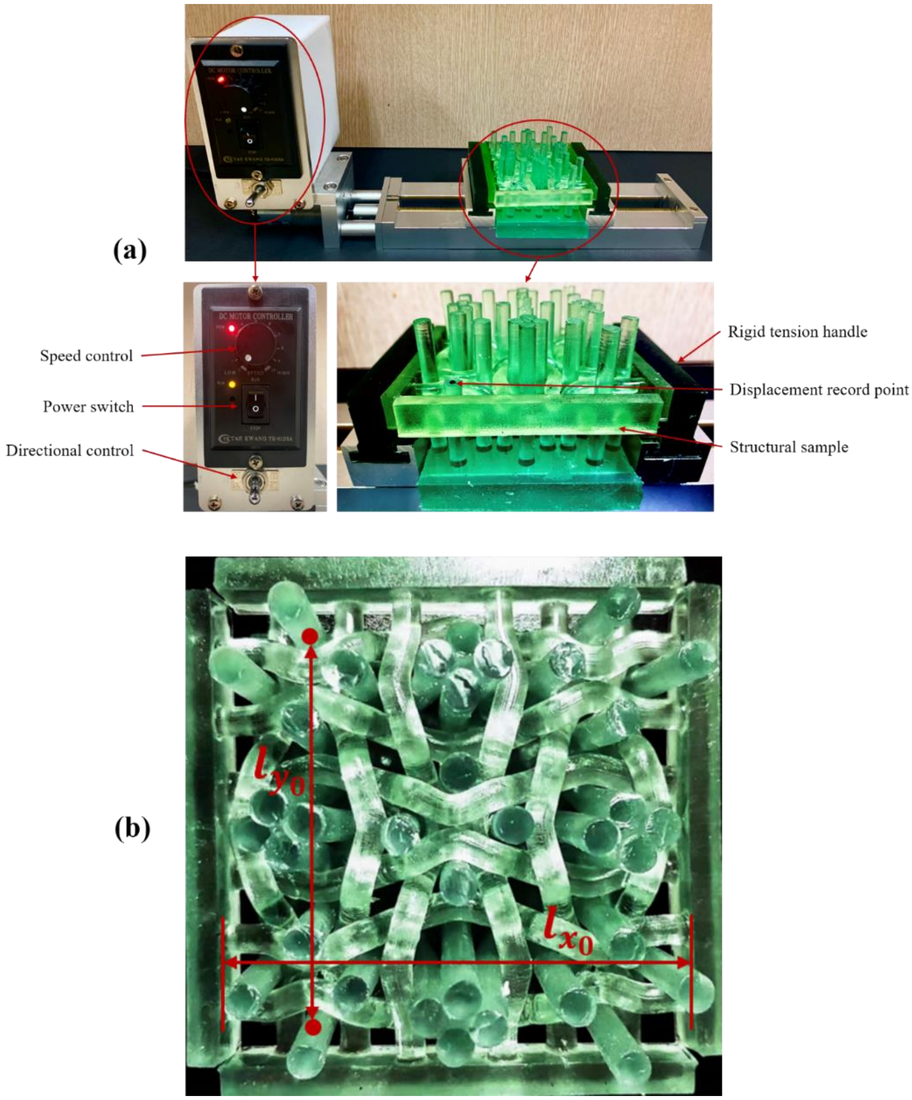

Figure 5. (a) Experimental setup of the stretching test and (b) one layer structure.

Chapter 4. Results and discussion

4.1 Experiments and simulation of 2D structure

The overall experimental deformation pattern obtained by stretching the 2D structure in the X direction by the stretching machine is shown in Figure 6(a). Compared with the structure before deformation in the Figure 5(b), it can be observed that the overall structure has increased strain in the Y direction, the fibers in the X- and Y-directions have changed from bending to straightening, the distortion of five unit one is obvious, and the four unit two patterns are almost unchanged. Through the deformation of unit one in the Figure 6(a), it can be seen that the fibers in the X and Y directions are separated, a gap is created in the middle, and all four Z-direction fibers move to the outside causing the overall unit one to increase in strain in the X and Y directions, showing auxetic deformation behavior. Therefore, the overall structure is deformed by the dominant structure of unit one when stretched in the X direction. Unit one has the auxetic behavior, and the deformation of unit two is not obvious, which leads to the increase of the overall 2D structure strain in both X and Y directions, showing the deformation behavior of auxetic.

The finite element simulation results of the X-direction fibers stretching by 4 mm are shown in Figure 6(b), and the deformation results obtained are the same as the experimental overall. Comparing the deformation results of the central unit one in the Figure 6(b), the separation of fibers in the X and Y directions and the movement of fibers in the Z direction to the outside are consistent with the deformation results of experiments received. The PR of the structure calculated from the measured displacement changes versus the X-direction fiber tensile displacement is shown in Figure 6(c). Results obtained from the finite element simulation and the experimental calculation are in good agreement. Also, PR curves in both conditions have the same trend with increasing stretching displacement in the X direction. During the stretching of 4 mm unit one strain continued to increase dominant deformation and the value of NPR continued to increase. However, the overall error in the data obtained from the experiments is large. This reason can be explained by the precise limitations of the vernier caliper measurements used for the experiments and the fact that the time was not perfectly accurate for 30 seconds. In addition, the PR of the finite element model vary more uniformly compared to the experimental results.

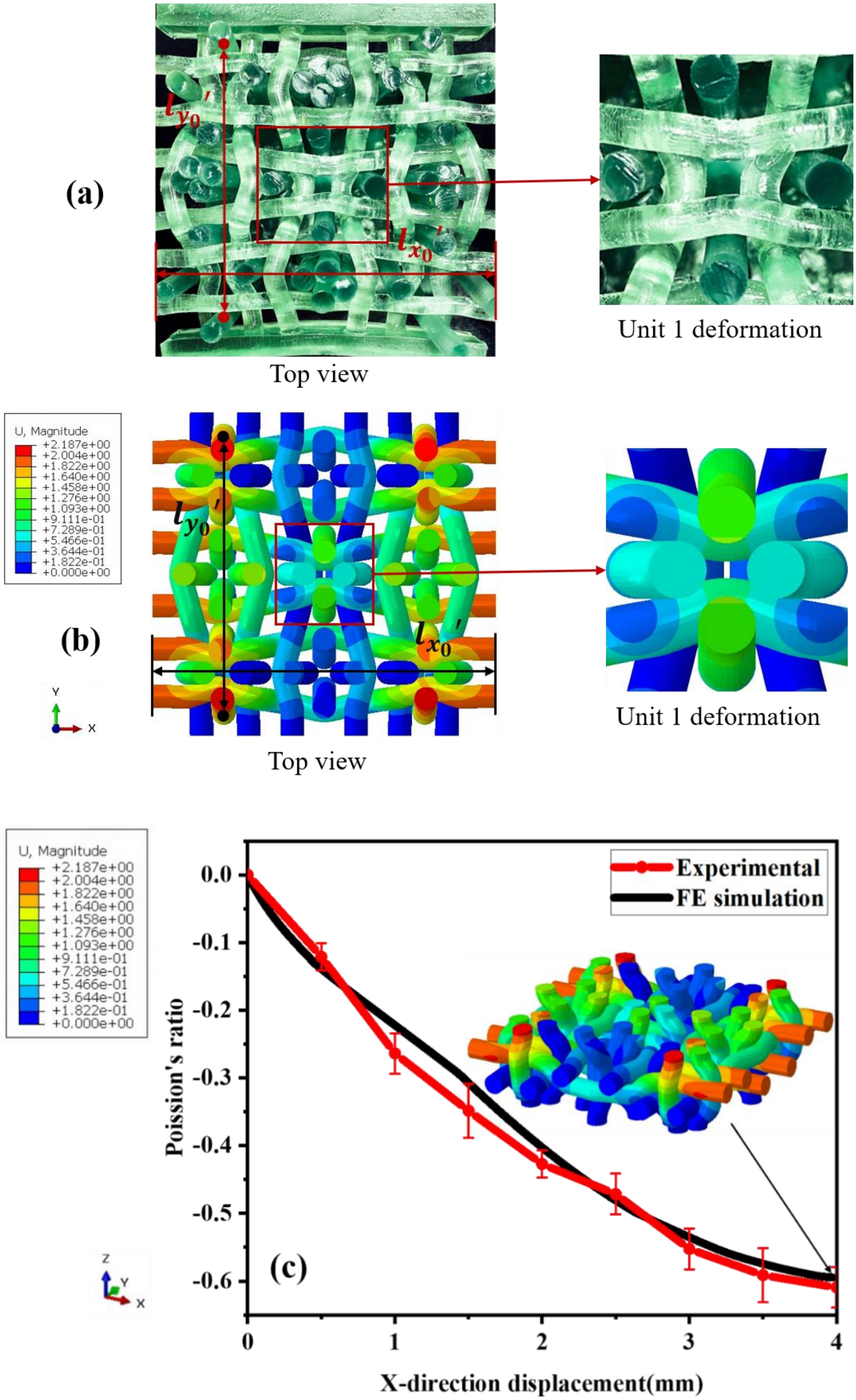
(a)
l_{y_0}'
l_{x_0}'
Top view
Unit 1 deformation
U, Magnitude
+2.187e+00
+2.004e+00
+1.822e+00
+1.640e+00
+1.458e+00
+1.276e+00
+1.093e+00
+9.111e-01
+7.289e-01
+5.466e-01
+3.644e-01
+1.822e-01
+0.000e+00
(b)
l_{y_0}'
l_{x_0}'
Top view
Unit 1 deformation
Y
X
U, Magnitude
+2.187e+00
+2.004e+00
+1.822e+00
+1.640e+00
+1.458e+00
+1.276e+00
+1.093e+00
+9.111e-01
+7.289e-01
+5.466e-01
+3.644e-01
+1.822e-01
+0.000e+00
Z
Y
X
Experimental
FE simulation
Poission's ratio
0.0
-0.1
-0.2
-0.3
-0.4
-0.5
-0.6
(c)
0
1
2
3
4
X-direction displacement(mm)

Figure 6. Deformation behavior of 2D structure with X-directional stretching. (a) A 2D structure and experimental deformation of Unit-1, (b) simulation results, and (c) comparison of simulated and measured Poisson's ratio according to X-directional displacements.

The integral structure of the Z-directional stretching experiment obtained using 150 mm long needles with unit two deformation are shown in Figure 7(a). In contrast to the original structure in Figure 5(b), there is almost no deformation in 5 unit one and clear deformation in 4 unit two. The overall structure has increased strain in the X and Y directions. Through the deformation diagram of unit two shown in Figure 7(a), it can be observed that the four Z-direction fibers, which were originally close together in the middle of unit two, are separated and a void is created in the center of the unit. At the same time, the X- and Y-direction fibers of unit two also move to the outside of the unit, respectively, resulting in an increase in strain in the X- and Y-directions of unit two, which exhibits an auxetic behavior. Therefore, in the Z-direction stretching, the 2D structure is deformed by the dominant structure of unit two, and unit one maintains the pre-deformation mode, showing the overall auxetic behavior. It is worth mentioning that the part with the largest overall strain in the Y direction is created between the X-direction fibers on the outside of the middle column unit one, which is used to calculate the value of PR. The FEA obtained deformation results as shown in Figure 7(b). There is a good resemblance with the experimental results, and the auxetic behavior can be confirmed regardless of the deformation of the overall single-layer one structure or unit two. Using the PR equation for the simulation results derived with the tensile displacement in the Z direction, the PR of the 2D structure varies as shown in Figure 7(c). The value of NPR at the beginning increases with the growth of tensile displacement, and unit two continues to dominate the deformation. At the tensile displacement of about 2.23 mm, the extreme value of NPR appears to be about -0.25, and then decreases slowly. This can be explained by the reason that the rate of variation of its displacement in the XY plane gradually decreases during the gradual straightening of the Z-direction fibers with respect to the rising tensile displacement. In addition, the strain in the XY plane will reach the maximum after the Z-direction fibers are completely straightened.

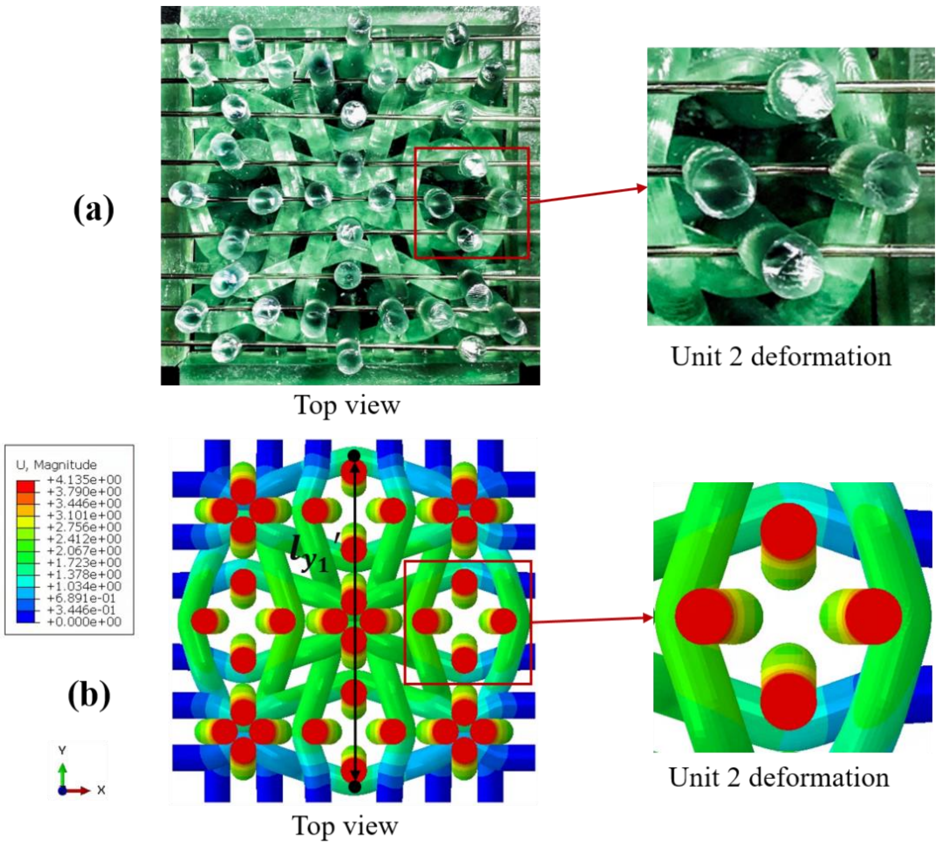

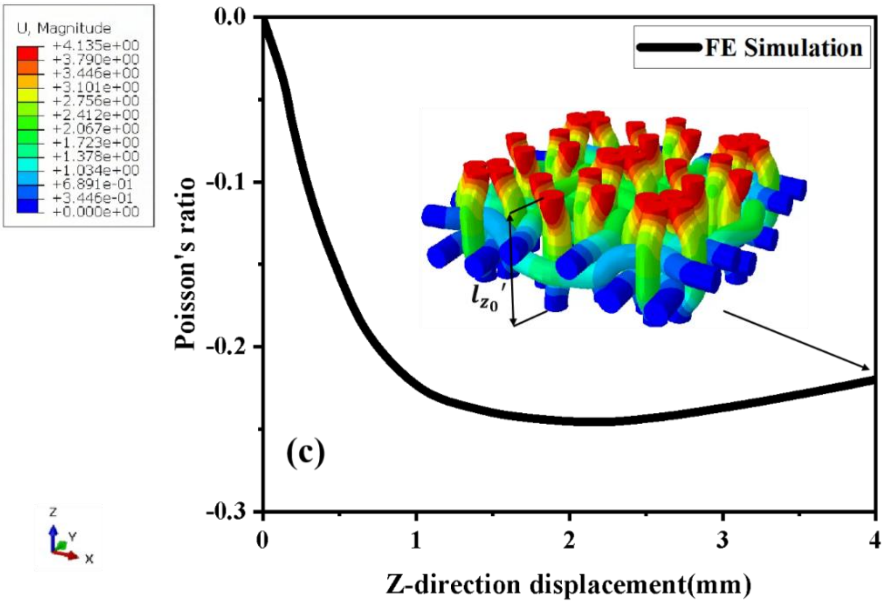

Figure 7. Deformation behavior of 2D structure with Z-directional stretching. (a) A 2D structure and Unit-2 deformation, (b) simulation results, and (c) comparison of simulated and measured Poisson's ratio according to Z-directional displacements.

In general, the experimental and simulation deformation results have good similarity in the 2D case. In other words, it is successfully demonstrated by experimental and FEA methods that the 2D structure has an auxetic deformation behavior when stretched in multiple directions.

4.2 FEM analysis and parametric study of 3D structure

The FEA method was used to investigate whether the 3D structure exhibited auxetic deformation behavior when stretched in multiple directions. Also, the effect of PR between the elastic modulus of the fiber itself and the tensile deformation of the structure was also discussed. The simulation results performed for the 3×3×4 model are shown in Figure 8(a), which demonstrates the deformation results of the layer one in the middle of the structure and the central unit one. There is a great degree of similarity with the deformation of 2D case in Figure 6(a,b). The X and Y direction fibers exhibit a tendency to be straightened. Observing the deformation of unit one in Figure 8(a)., the X- and Y-direction fibers are separated and a gap is created in the center, showing an auxetic deformation in the XY plane. The PR values calculated for the material properties "elastic" and "isotropy" with Young's modulus of 50 MPa, 100 MPa and 200 MPa are shown in Figure 8(b). The PR values are identical with stretching in the X direction, that is, the Young's modulus of the elastic material properties is independent of the magnitude of the PR of the structure, which exhibits only one PR change. Compared to the results of the PR values for the 2D case in Figure 6(c), the NPR values for the 3D case are smaller for the same tensile displacement. This can be explained by the fact that units, which are connected to the top and bottom of unit one, plays a limiting role for the deformation of the fibers in the Z-direction in unit one.

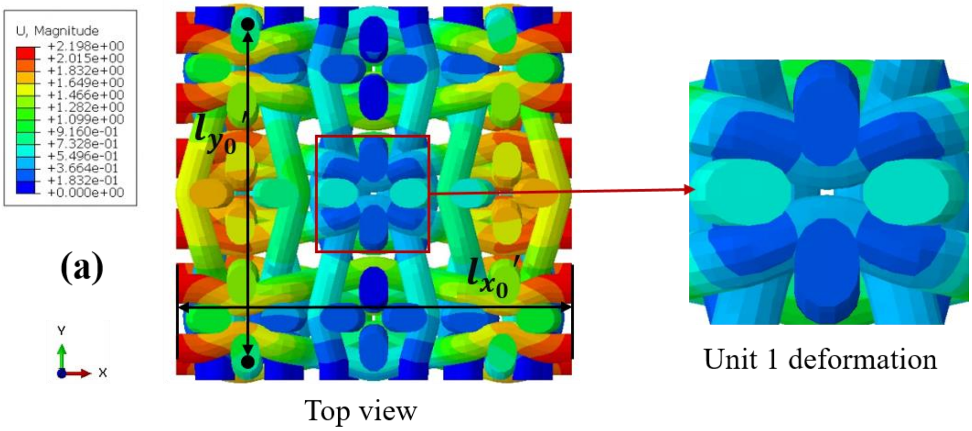

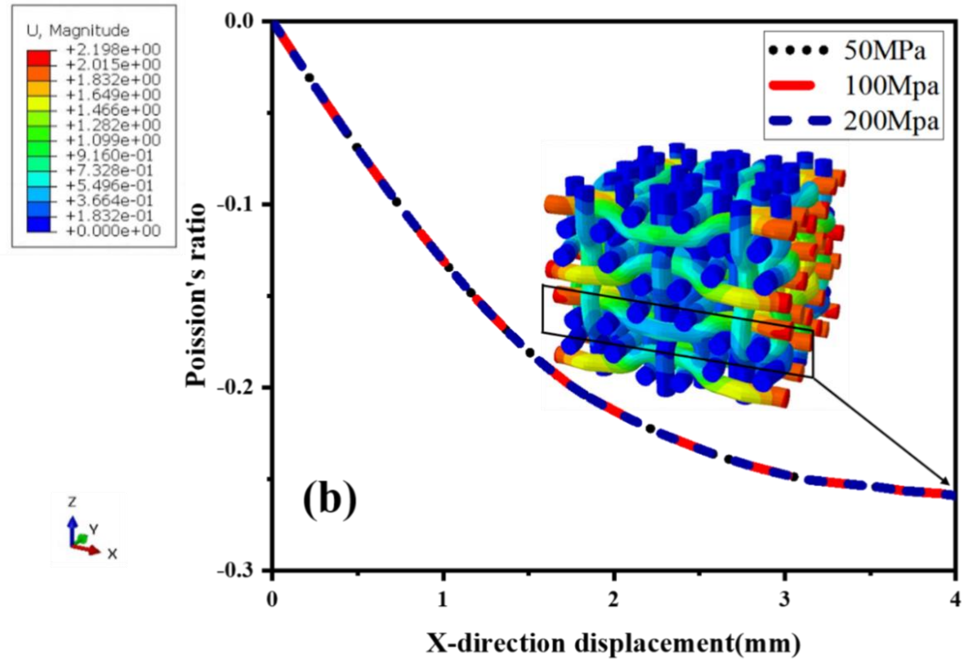

Figure 8. Deformation behavior of 3D structure with X-directional stretching. (a) A 3D structure and simulated Unit-1 deformation and (b) simulated Poisson's ratio according to displacement in the X-direction.

Similarly, Z-direction stretching deformation results for the 3D structure are shown in Figure 9(a), which also has a good similarity with the 2D structure deformation in Figure 7(a and b). In the 3D case, the deformed layer one structure has increased strain in the X and Y directions. Among them, the deformation of unit two is obvious, and the separation of the four central Z-direction fibers produces voids and shows auxetic deformation of unit two result as shown in Figure 9(a). The relationship between PR and stretching displacement obtained for varying the modulus of elasticity (50 MPa, 100 MPa and 200 MPa) is shown in Figure 9(b). The NPR values are also identical, but the 3D structure has a significantly larger NPR when stretched in the Z direction compared to the results of 2D case in Figure 7(c). The main reason is that there is a height difference of about 4 times between the 3D structure and the 2D structure, so the Z-direction of the 3D structure changes less under the same displacement of stretching. And the Z-direction fibers start to change strongly in response to the displacement in the XY plane, which leads to a certain degree of increase in the NPR value.

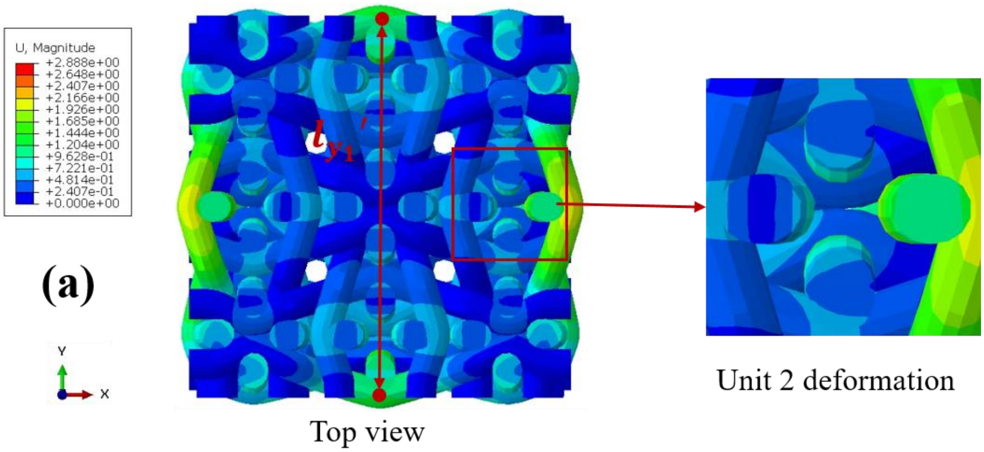

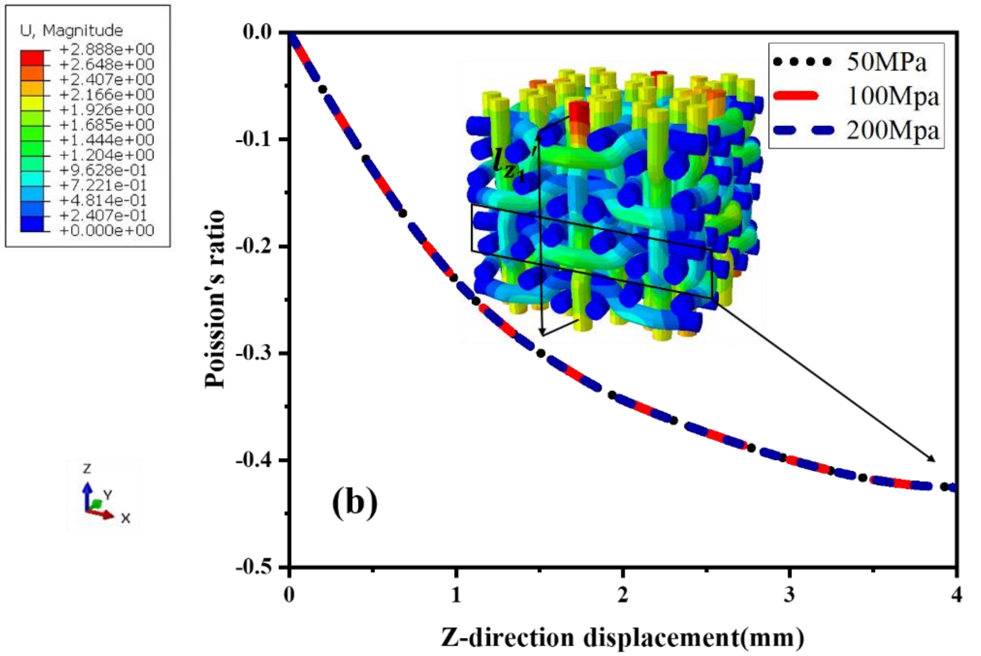

Figure 9. Deformation behavior of 3D structure with Z-directional stretching. (a) A 3D structure and simulated Unit-2 deformation and (b) simulated Poisson's ratio according to displacement in the Z-direction.

Overall, the FEA method effectively illustrates the auxetic behavior of the 3D structure when stretched in multiple directions, and the modulus of the fiber itself has no effect on the NPR behavior of the structure.

In order to achieve the required degree of auxetic for 3D structures and to achieve some control over the NPR value of the structure, the influence of geometric parameters was investigated. That is, the deformation behavior of the structure with different diameter ratios was simulated by means of FEA. Altering the ratio of fiber diameter in the X and Y directions to fiber diameter in the Z direction ΦX (4 mm): ΦZ (5 mm) = 0.8:1 for stretching in the X and Z directions results in the simulated deformation as shown in Figure 10(a), and ΦX (6 mm): ΦZ (5 mm) = 1.2:1 results as shown in Figure 10(b). In comparison with the deformation results of the third layer in Figure 10(a) and Figure 10(b), although the internal layer structure shows similar deformation trends and the deformation of the NPR is confirmed in both the X and Z directions of stretching, there are still some differences when comparing the deformation of the units in both. In particular, unit one in Figure 10(a) is more deformed than unit one in Figure 10(b), and the separation of X- and Y-directions fibers and the gap in the center are more obvious. In contrast, unit one in Figure 10(a) is not deformed as much as unit two in Figure 10(b), and the degree of four Z-direction fiber separation and the auxetic behavior of unit two are slightly less. Figure 10(c) shows the NPR results with different diameter ratios at the same X-directional stretching displacement. It can be found that the NPR behavior achieved by the 3D structure becomes less pronounced with larger values of ΦX:ΦZ. This is logical since the diameter ratio of the fibers determines the original degree of bending of the fibers in each direction. The larger the value of ΦX:ΦZ, the smaller the original bending of the fibers in the X and Y directions, so the smaller the gap in the middle of the unit resulting from the straightening of the fibers in the X direction when the same displacement is stretched in the X direction, which leads to the less obvious auxetic behavior of the overall structure. On the contrary, if the value of ΦX:ΦZ is larger in the Z-direction stretching, the original bending of the fibers in the Z direction will be larger and the auxetic behavior achieved by the 3D structure will be more obvious as shown in Figure 10(d). This also effectively explains the differences in deformation between Figure 10(a) and 10(b) at the same time. In general, the results indicate that the extent of NPR behavior in different directions of the structure can be achieved by variating the diameter ratio of the fibers.

(a)

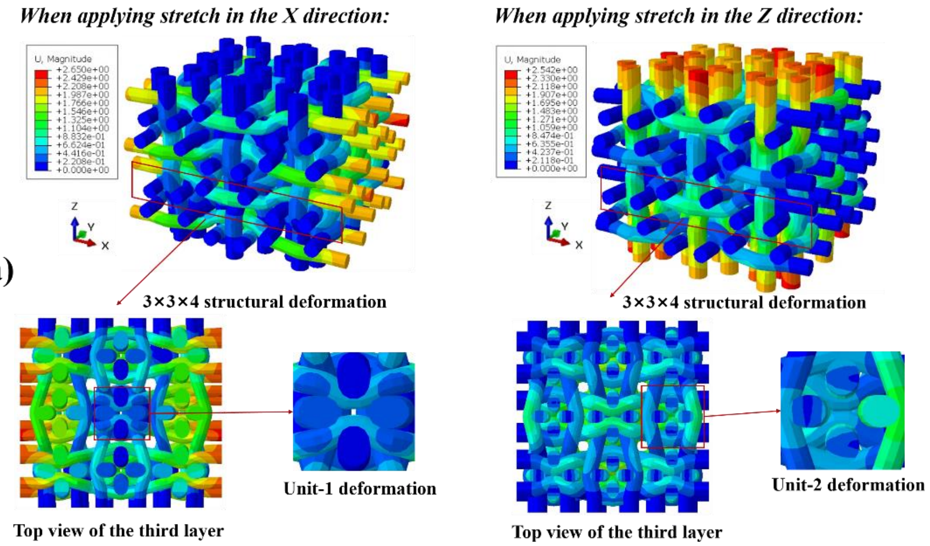

ΦX (4mm) : ΦZ (5mm)= 0.8 : 1

(b)

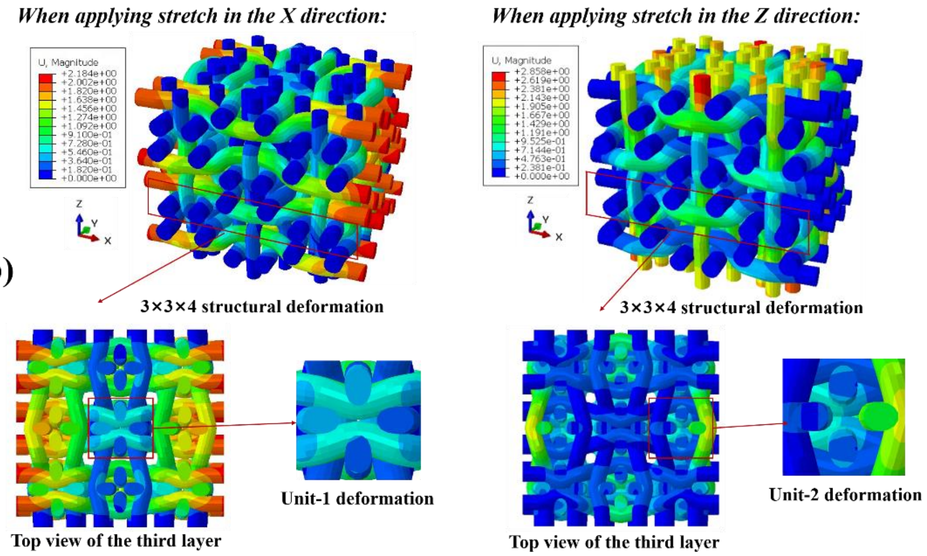

ΦX (6mm) : ΦZ (5mm)= 1.2 : 1

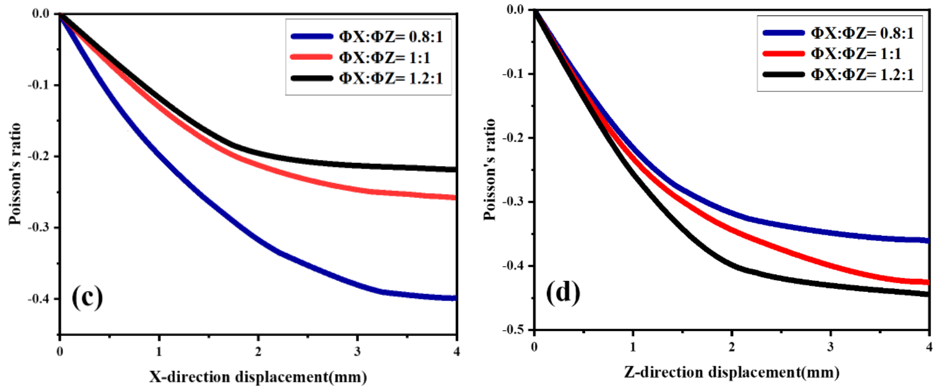

Figure 10. Simulated deformation behavior of 3D structure with X- and Z-directional stretching when (a) ΦX(4 mm): ΦZ(5 mm) = 0.8:1, (b) ΦX(6 mm): ΦZ(5 mm) = 1.2:1. FE simulation of the measured PR with variation in the diameter ratio on stretching displacement (c) in the X and (d) Z directions.

4.3 Simulation of impact resistance performance

After demonstrating the multi-directional NPR behavior of the structure, this paper uses finite element analysis methods to predict the potential applications of multi-directional auxetic materials. Using a rigid body breakdown disc model, there is discussion of whether such materials have the potential to outperform conventional materials in terms of impact resistance performance. In this study, the auxetic structure is homogenized by assigning the average value of PR of the 3D structure to the homogenized model itself and taking its opposite as a comparison for impact simulation experiments. As shown in the Figure 11, a rigid flat-head cylinder with a diameter of 24 mm and a disc with a diameter of 100 mm, thickness of 10 mm are created in ABAQUS software. The mass of the rigid body is 0.1 kg, and the elastic modulus of the disc is set to 50MPa. Where, the initial distance between the rigid body and the disc is 10 mm. Then with maximum strain 0.4 as the damage criterion, the disc is annular clamping and the rigid body is given 1 mm/s initial velocity as the boundary condition. Finally, Dynamic, Explicit analysis is performed for both positive Poisson's ratio (PPR) and NPR structures. In addition, the energy loss is calculated based on the velocity change before and after the rigid body strikes the disc, and used to characterize the impact resistance performance. That is, $E = \frac{1}{2}mV_0^2 - \frac{1}{2}mV_1^2$, where E is the energy damage, m is the mass of the rigid body, V_0 is the initial velocity of the rigid body, and V_1 is the instantaneous velocity.

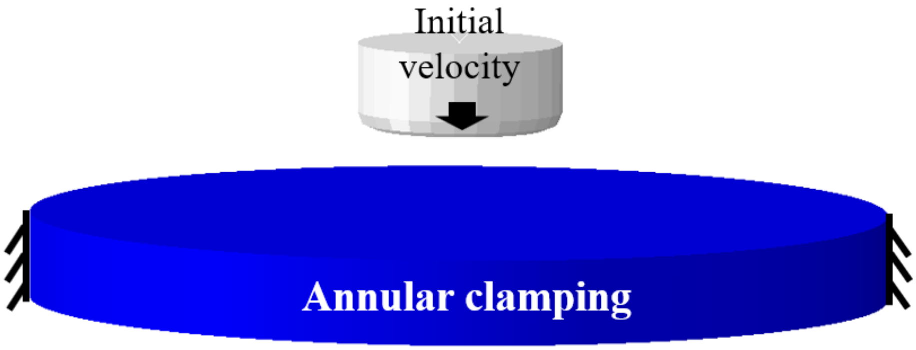

Figure 11. Model geometry for simulated impacts.

The average value of PR -0.3428 in each direction of the 3D structure was assigned to the homogenized model and its opposite number 0.3428 was used as the PPR model for the comparative impact finite element analysis. Figure 12 shows the views of the PPR and NPR models after being struck by the rigid body. It can be observed that the damage of the PPR model is concentrated, and the stresses are concentrated around the rigid body. On the contrary, the damage of the NPR model is scattered and the stresses are evenly distributed. Figure 13(a) plots the velocity versus displacement of the rigid body strike. The energy damage calculated from the velocity is shown in Figure 13(b), while Figure 13(c) also shows the four identified characteristic events and their associated damage patterns presented in cross-sectional view for each of the PPR and NPR models during the impact. Figure 13 shows the rigid body energy loss process, indicating a rapid increase in energy loss at the time of initial contact with the disc model (event 1), followed by a decrease in the rate of energy loss due to damage occurring in the disc due to the maximum strain criterion (event 2). In particular, the main part of the PPR model that starts to suffer damage is the surface in contact with the rigid body, and the NPR is the bottom of the model. As the rigid body continues to move, cracking occurs at the bottom of the PPR disc model and damage occurs on the surface of the NPR model in contact with the rigid body leading to slightly increased fluctuations in the rate of energy damage (event 3). Eventually, until the breakdown process is completed (event 4).

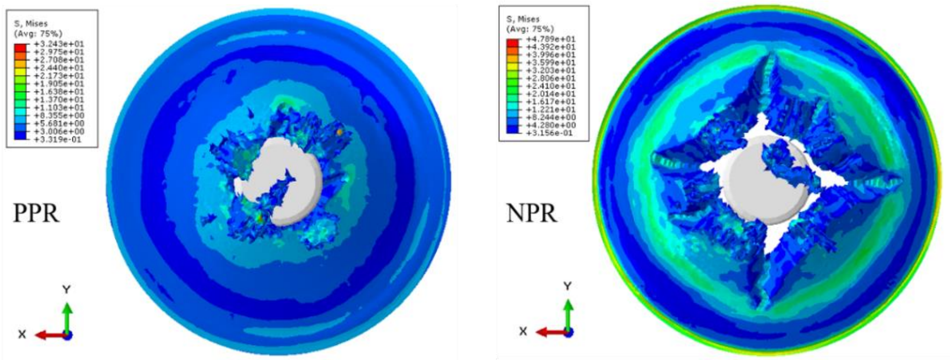

Figure 12. Results after PPR and NPR rigid body breakdown models.

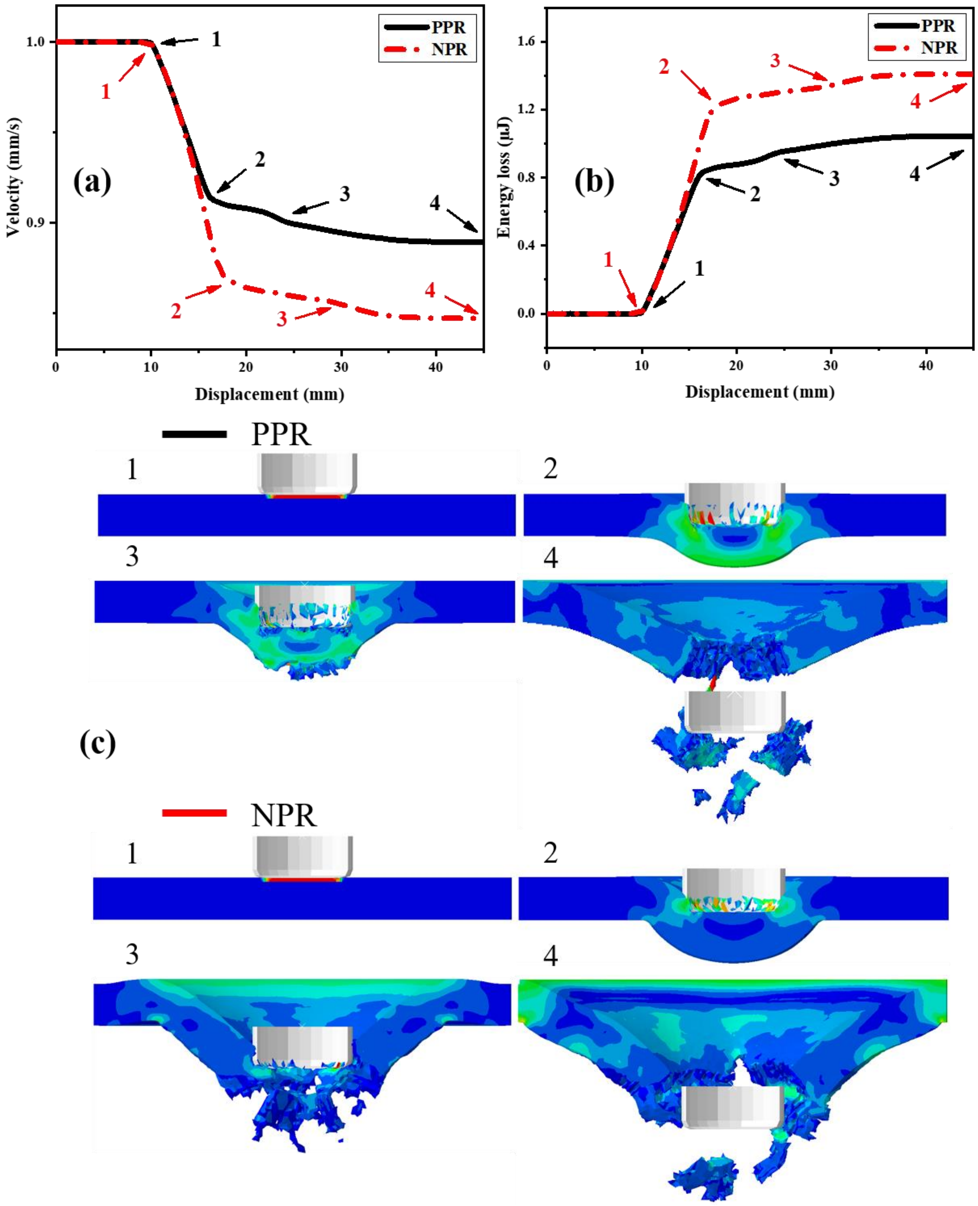

Figure 13. During rigid body impact processes, both PPR and NPR models results of the relationship between the rigid body displacement and (a)velocity, (b)energy loss, (c)schematic diagram of the model for special events.

For the evolution of the impact process of the two models, it is shown that the PPR model mainly strains at the site of the force, while the NPR model can disperse the force and distribute it evenly after the force is applied. Also, the NPR model has a faster stiffener energy damage rate compared to the PPR model, and the required stiffener displacement for the model to produce damage is farther. The rigid body velocity decreases more after the breakdown and the overall energy loss is larger. These observations reveal that the NPR material outperforms the PPR material in terms of impact force resistance under equivalent elastic modulus, and damage conditions.

Chapter 4. Conclusion

The 3D auxetic woven structure was created by designing the connection of special compilation units. Then the experimental method of 3D printing and FEA simulations were applied to investigate the auxetic behavior and deformation mechanism of the structure when stretched in each direction. The factors affecting the NPR deformation of the designed structure were explored for varying different elastic modulus and fiber diameter ratios in different directions. Also, the impact resistance application potential of the auxetic structure was examined with a rigid body breakdown disc model. From the study, these conclusions can be drawn.

1) The simulation results for the 2D case are in good agreement with the experimental results, providing confidence in proving the multi-directional auxetic deformation of the 3D structure.

2) FEA of the 3D structure shows that single fibers can achieve multi-directional auxetic properties of the overall structure by special weaving methods in 3D.

3) The modulus of elasticity of the fiber has no effect on the NPR of the structure, but the diameter ratios of the fibers in different directions have a great influence on the tensile behavior of the structure. To achieve greater auxetic deformation in a particular direction, this can be achieved by changing the diameter ratio.

4) Compared to conventional materials, the multi-directional auxetic

material has great potential for impact resistance applications.

Reference

[1] Babaee, S., et al., *3D soft metamaterials with negative Poisson's ratio.* Advanced Materials, 2013. **25**(36): p. 5044-5049.

[2] Hou, S., et al., *Mechanical properties of sandwich composites with 3d-printed auxetic and non-auxetic lattice cores under low velocity impact.* Materials & Design, 2018. **160**: p. 1305-1321.

[3] Madke, R.R. and R. Chowdhury, *Anti-impact behavior of auxetic sandwich structure with braided face sheets and 3D re-entrant cores.* Composite Structures, 2020. **236**: p. 111838.

[4] Scarpa, F., L. Ciffo, and J. Yates, *Dynamic properties of high structural integrity auxetic open cell foam.* Smart Materials and Structures, 2003. **13**(1): p. 49.

[5] Novak, N., et al., *Blast response study of the sandwich composite panels with 3D chiral auxetic core.* Composite Structures, 2019. **210**: p. 167-178.

[6] Choi, J. and R. Lakes, *Non-linear properties of polymer cellular materials with a negative Poisson's ratio.* Journal of Materials Science, 1992. **27**(17): p. 4678-4684.

[7] Peng, X.-L. and S. Bargmann, *A novel hybrid-honeycomb structure: Enhanced stiffness, tunable auxeticity and negative thermal expansion.* International Journal of Mechanical Sciences, 2021. **190**: p. 106021.

[8] Ai, L. and X.-L. Gao, *Three-dimensional metamaterials with a negative Poisson's ratio and a non-positive coefficient of thermal expansion.* International Journal of Mechanical Sciences, 2018. **135**: p. 101-113.

[9] Liu, Y. and H. Hu, *A review on auxetic structures and polymeric materials.* Scientific research and essays, 2010. **5**(10): p. 1052-1063.

[10] Lira, C., F. Scarpa, and R. Rajasekaran, *A gradient cellular core for aeroengine fan blades based on auxetic configurations.* Journal of Intelligent Material Systems and Structures, 2011. **22**(9): p. 907-917.

[11] Yao, Y., et al., *Fabrication and characterization of auxetic shape memory composite foams.* Composites Part B: Engineering, 2018. **152**: p. 1-7.

[12] Ali, M.N., J.J. Busfield, and I.U. Rehman, *Auxetic oesophageal stents: structure and mechanical properties.* Journal of Materials Science: Materials in Medicine, 2014. **25**(2): p. 527-553.

[13] Xu, B., et al., *Making negative Poisson's ratio microstructures by soft lithography.* Advanced materials, 1999. **11**(14): p. 1186-1189.

[14] Foster, L., et al., *Application of auxetic foam in sports helmets.* Applied Sciences, 2018. **8**(3): p. 354.

[15] Gibson, L.J., et al., *The mechanics of two-dimensional cellular materials.* Proceedings of the Royal Society of London. A. Mathematical and Physical Sciences, 1982. **382**(1782): p. 25-42.

[16] Zhang, X.G., et al., *A novel auxetic chiral lattice composite: Experimental and numerical study.* Composite Structures, 2022. **282**: p. 115043.

[17] Mizzi, L., et al., *Influence of translational disorder on the mechanical properties of hexachiral honeycomb systems.* Composites Part B: Engineering, 2015. **80**: p. 84-91.
[18] Grima, J.N. and K.E. Evans, *Auxetic behavior from rotating triangles.* Journal of materials science, 2006. **41**(10): p. 3193-3196.
[19] Quan, C., et al., *3d printed continuous fiber reinforced composite auxetic honeycomb structures.* Composites Part B: Engineering, 2020. **187**: p. 107858.
[20] Qi, C., et al., *Quasi-static crushing behavior of novel re-entrant circular auxetic honeycombs.* Composites Part B: Engineering, 2020. **197**: p. 108117.
[21] Grima, J.N., et al., *Auxetic behaviour from rotating semi-rigid units.* physica status solidi (b), 2007. **244**(3): p. 866-882.
[22] Zhang, M., et al., *Three-dimensional composites with nearly isotropic negative Poisson's ratio by random inclusions: Experiments and finite element simulation.* Composites Science and Technology, 2022. **218**: p. 109195.
[23] Grima, J.N., et al., *Auxetic behaviour in non-crystalline materials having star or triangular shaped perforations.* Journal of Non-Crystalline Solids, 2010. **356**(37-40): p. 1980-1987.
[24] Attard, D. and J.N. Grima, *Auxetic behaviour from rotating rhombi.* physica status solidi (b), 2008. **245**(11): p. 2395-2404.
[25] Grima, J.N., et al., *On the auxetic properties of rotating rhombi and parallelograms: A preliminary investigation.* physica status solidi (b), 2008. **245**(3): p. 521-529.
[26] Assidi, M. and J.-F. Ganghoffer, *Composites with auxetic inclusions showing both an auxetic behavior and enhancement of their mechanical properties.* Composite Structures, 2012. **94**(8): p. 2373-2382.
[27] Kochmann, D.M. and G.N. Venturini, *Homogenized mechanical properties of auxetic composite materials in finite-strain elasticity.* Smart materials and structures, 2013. **22**(8): p. 084004.
[28] Herakovich, C.T., *Composite laminates with negative through-the-thickness Poisson's ratios.* Journal of Composite Materials, 1984. **18**(5): p. 447-455.
[29] Evans, K., J. Donoghue, and K. Alderson, *The design, matching and manufacture of auxetic carbon fibre laminates.* Journal of composite materials, 2004. **38**(2): p. 95-106.
[30] Alderson, K., et al., *How to make auxetic fibre reinforced composites.* physica status solidi (b), 2005. **242**(3): p. 509-518.
[31] Zhang, R., H.-L. Yeh, and H.-Y. Yeh, *A preliminary study of negative Poisson's ratio of laminated fiber reinforced composites.* Journal of reinforced plastics and composites, 1998. **17**(18): p. 1651-1664.
[32] Alderson, K. and V. Coenen, *The low velocity impact response of auxetic carbon fibre laminates.* physica status solidi (b), 2008. **245**(3): p. 489-496.

[33] Miller, W., et al., *The manufacture and characterisation of a novel, low modulus, negative Poisson’s ratio composite.* Composites Science and Technology, 2009. **69**(5): p. 651-655.
[34] Ge, Z. and H. Hu, *Innovative three-dimensional fabric structure with negative Poisson's ratio for composite reinforcement.* Textile Research Journal, 2013. **83**(5): p. 543-550.
[35] Ge, Z., H. Hu, and Y. Liu, *A finite element analysis of a 3D auxetic textile structure for composite reinforcement.* Smart materials and structures, 2013. **22**(8): p. 084005.
[36] Ge, Z., H. Hu, and Y. Liu, *Numerical analysis of deformation behavior of a 3D textile structure with negative Poisson’s ratio under compression.* Textile Research Journal, 2015. **85**(5): p. 548-557.
[37] Jiang, L., B. Gu, and H. Hu, *Auxetic composite made with multilayer orthogonal structural reinforcement.* Composite Structures, 2016. **135**: p. 23-29.
[38] Ahmed, H.I., et al., *Development of 3D auxetic structures using para-aramid and ultra-high molecular weight polyethylene yarns.* The Journal of The Textile Institute, 2021. **112**(9): p. 1417-1427.
[39] Yang, C.-C., T. Ngo, and P. Tran, *Influences of weaving architectures on the impact resistance of multi-layer fabrics.* Materials & Design, 2015. **85**: p. 282-295.

Korean abstract

직조 섬유 구조로 강화된 오그제틱(Auxetic) 복합 재료에 대한 논의는 최근까지 단방향 장력 또는 압축에 초점을 맞추었으며, 종종 구조에서 다른 역할을 하기 위해 여러 개의 섬유가 필요했기에 실제 응용 분야에서 오그제틱 재료의 장점을 완벽하게 활용하기 어렵다. 우리는 이 연구에서 여러 방향으로 늘어나 오그제틱 거동을 할 수 있는 직조 구조를 제시한다. 단일 레이어 구조는 3차원(3D) 프린팅 방법을 통해 성공적으로 제작되었으며 유한 요소 해석(FEA)을 통해 비교했다. 또한, 3D 구조의 다방향 인장 변형 거동을 시뮬레이션하여 단층 구조와 3D 구조의 포아송의 비율(PR) 값을 구했다. 추가로, 구조물의 보조적 행동에 영향을 미치는 요소들을 논의했다. 그 결과, 실험과 FEA 결과가 좋은 유사성을 가지며 구조가 세 방향으로 모두 늘어나면 오그제틱 동작을 달성할 수 있음을 확인했다. 특히, 각 방향의 섬유의 직경비는 구조물의 오그제틱 변형 정도에 영향을 미치는 요인이다. 이 연구는 다방향 오그제틱 섬유 복합체의 개발에 대한 새로운 접근법을 제공한다. 또한, 충격 저항 성능 응용을 위한 다방향 오그제틱 재료의 잠재력을 발견하였다.

핵심어: 오그제틱(Auxetic) 직물 구조, 유한 요소 해석, 다차원 오그제틱 변형, 3D 프린팅, 내충격성

학번: 2020-27841